Recombination in Highly Injected Silicon

RONALD A. SINTON AND RICHARD M. SWANSON, MEMBER, IEEE

Abstract—**Recent advances in solar cells designed to operate under high-level injection conditions have produced devices that are approaching some of the limits imposed by the fundamental band-to-band Auger recombination in silicon. A device has been optimized to study this recombination by using the fabrication technology developed for point-contact solar cells. Using both steady-state and transient measurements, the recombination rates in high-resistivity Si in the injected carrier density range of 10^{15} to 2×10^{17} carriers/cm^3 were investigated. The coefficient of the recombination, which depends on the carrier density cubed, is found to be 1.66×10^{-30} cm^6/s $\pm$ 15 percent. This result is four times higher than the ambipolar Auger coefficient commonly used in the modeling of devices that operate in this injected carrier density range and lowers the expected limit efficiencies for silicon solar cells.**

I. Introduction

As silicon material and processing techniques improve, the ultimate efficiencies of Si solar cells are expected to be limited by the bulk Auger recombination [1], [2]. Under high-level injection conditions, this recombination has a characteristic signature, due to its dependence on the cube of the carrier density, and has been observed in the best demonstrated Si concentrator solar cells. These cells are made from high-resistivity silicon but are conductivity modulated to carrier densities greater than 10^{17}/cm^3 by the photogeneration under concentrated sunlight. A comparison of the modeling predictions to the short-circuit current versus incident illumination intensity data was previously found to be poor unless the Auger recombination coefficients are increased by a factor of 3 or 4 over the commonly accepted values in the relevant range of carrier densities, up to 10^{17}/cm^3 [3]. In this paper we show that such a modification is also necessary to account for the illuminated open-circuit voltage and the open-circuit voltage decay.

The most widely used values for the Auger coefficients are those measured by Dziewior and Schmid in heavily doped silicon and Svantesson and Nilsson in highly injected silicon [4], [5]. These coefficients are in good agreement, 3.8 and 3.88×10^{-31} cm^6/s, respectively, if the ambipolar coefficient is taken to be the sum of the individual coefficients in p-type and n-type silicon. Both of these experiments determined the recombination rates primarily at carrier densities above 10^{18} carriers/cm^3 where this recombination clearly dominates over the other recombination processes. Other authors have observed an apparent increase in the coefficient of this recombination at carrier densities less than 10^{18} [6]–[8]. Most of these results involved a subtraction of other comparable recombination components in the analysis for this range in carrier density except for the most recent results on unprocessed Si. One of these experiments measured the high injection lifetimes by utilizing high-resistivity wafers that were screened for unusually long bulk lifetime. The surface recombination was reduced to extremely low levels by immersion in acids [9]. Other authors have measured the lifetimes in float-zone doped material either in the boule or in thick wafers [10], [11].

In this study, we have optimized a device specifically to study the lifetimes under high-level injection conditions in processed silicon by utilizing the observed sensitivity of high-efficiency concentrator solar cells to this parasitic recombination component. We designed and fabricated a test structure that can determine the coefficient of this process by focusing on a special case for which the analysis is vastly simplified, and this recombination is dominant. Such a device can be constructed so that the analysis is insensitive to the modeling parameters such as the diffusion coefficients.

II. Method

The method chosen to characterize the Auger recombination was to monitor the open-circuit voltage of a high-injected solar cell under both steady-state conditions, using a measurement of V_{oc} versus the incident illumination intensities, and transient conditions, by observing the open-circuit voltage decay (OCVD). Point-contact solar cells of the configuration shown in Fig. 1 have shown a sensitivity to the Auger recombination. Since this recombination produces a parasitic loss in solar cell efficiency, a well designed solar cell will necessarily minimize this effect. A detailed model of this solar cell has arisen from this effort [13]. Using this model, the opposite effect can be achieved, that is, to *maximize* the sensitivity to this recombination. This is the approach described here.

Consider the special case of a solar cell under open-circuit voltage conditions. The photogenerated carriers per unit of cell area J_{ph} are balanced by the recombination R as well as the change in carrier density, both expressed as charge

$$J_{ph} = q \int \left(\frac{dn}{dt}\right) dx + q \int R\, dx. \qquad (1)$$

Manuscript received September 26, 1986; revised January 15, 1987. The devices reported on in this work were fabricated in association with the Stanford Integrated Circuits Laboratory Research Institute under Contract RP-790-2 and under an Exxon Fellowship.

The authors are with the Stanford Electronics Laboratories, Stanford, CA 94305.

IEEE Log Number 8613909.

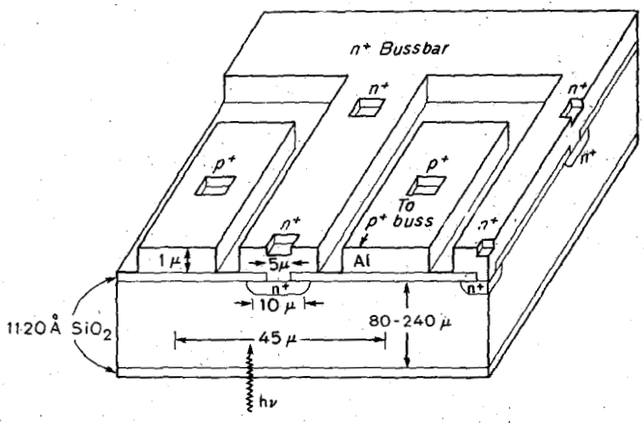

Fig. 1. A cross section of a portion of a point contact solar cell near the main bussbar for the n^+ diffusions [12].

TABLE I
VARIABLES

J_{ph}	Total photogenerated current
V_{oc}	Open Circuit Voltage
R	Recombination rate (carriers/volume)
τ	Shockley-Read-Hall high-level injection lifetime
n	Carrier density, n=p in high level injection
n_{on}, n_{op}	n at the depletion edge of the n^+/p^+ diffusion.
S	Surface recombination velocity
J_{on}/J_{op}	Emitter saturation current density for the n^+/p^+ diffusion
A_n/A_p	Fraction of the total back surface area covered by n^+/p^+ diffusion
C_A	Ambipolar Auger coefficient
W	Solar cell wafer thickness
D_A	Ambipolar diffusion coefficient
r_1	Boundary between 1-dimensional and 3-dimensional regions.
r_{on}/r_{op}	Radius of a hemisphere of equivalent area to the experimental square diffusion.
n_1	The carrier density at r_1
Δn	The drop in carrier density across the 3-dimensional region near the n or p-type diffusion

In the illuminated steady-state case, this equality becomes [13]

$$J_{ph} = \frac{q}{\tau}\int n(x)\,dx + qS(n_f + n_b) + J_{on}A_n\left(\frac{n_{on}}{n_i}\right)^2 + J_{op}A_p\left(\frac{n_{op}}{n_i}\right)^2 + qC_a\int n^3(x)\,dx \qquad (2)$$

for the highly injected case where $n = p >> N_B$, the background doping level. A list of the variables in (2) is given in Table I. In this equation, the first term represents the bulk Shockley-Read-Hall recombination, the second is the surface recombination, the third and fourth account for diffused region recombination, and the last is the bulk Auger recombination.

In conjunction with a high injection solar cell model [13] that can predict $n(x)$, (2) can be used to find the coefficients in a self-consistent manner. The photogenerated current J_{ph} can be accurately determined from the short-circuit current of solar cells at low illumination intensities where the quantum efficiency is nearly unity (a correction, less than 1.0 percent, can be made from the modeling). Notice that if $n(x)$ is uniform across the wafer, (2) is vastly simplified. The measurement then becomes entirely model independent since n is determined by the measured open-circuit terminal voltage [13].

$$V_{oc} = \frac{kT}{q}\ln\left(\frac{n_{on}n_{op}}{n_i^2}\right) \quad \text{or} \quad n = n_i \exp\frac{qV_{oc}}{2kT}. \qquad (3)$$

This idealized case is approached if the diffusion length is much greater than the cell thickness as long as the surface and emitter recombination rates are much smaller than in the diffusion-limited case.

The device reported here was designed with this in mind. The optimization involved two goals:

1) All of the recombination components that are technology dependent (the bulk, surface, and emitter (diffused region)), should be reduced to the lowest possible levels to maximize the sensitivity of the measurement to the Auger recombination.

2) The carrier density should be as uniform as possible so that the modeling correction is very small to insure the most accurate extraction of C_A.

The first two terms in (2) were minimized by using processing techniques that have been developed for the demonstrated solar cells. It has been shown that lifetimes greater than several milliseconds and surface recombination velocities less than 10 cm/s can be achieved on pro-

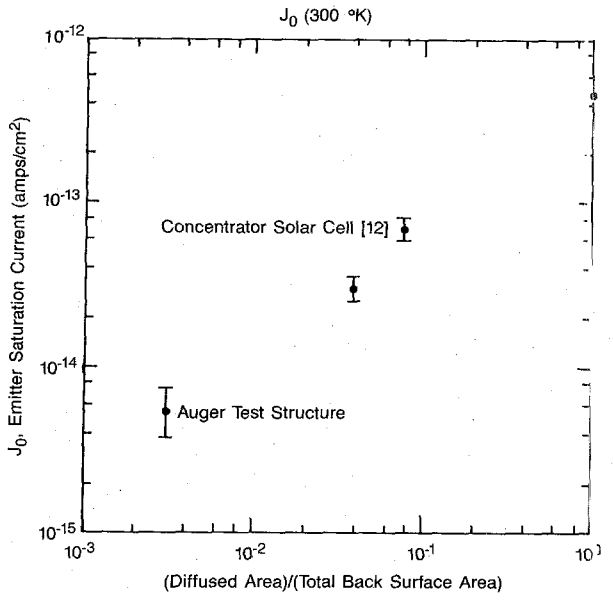

Fig. 2. The experimental emitter saturation currents of point contact cells averaged over the entire back surface area of the cells.

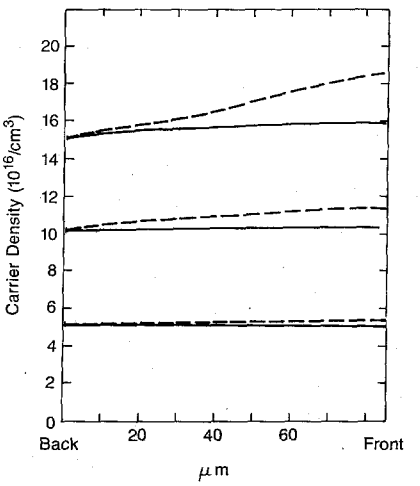

Fig. 3. The carrier density as a function of position in a point contact cell under illuminated open-circuit conditions along a line from the front of the cell to a p^+ region at the back of the cell. The contact coverage fractions are $A_n = A_p = 0.1$ for the dashed curve, and optimized solar cell, and 0.0025 for the solid curve, an Auger test structure.

cessed wafers [3]. The second and third terms can be reduced to arbitrarily small levels by reducing the areas of the diffusions, A_n and A_p. This is demonstrated in Fig. 2 where an effective emitter saturation current is plotted as a function of the total back surface area coverage fraction of the diffused regions. This effective emitter saturation current J_{eff} is that which would be found by replacing the emitter terms, the third and fourth terms in (2), with $J_{\text{eff}}(n/n_i)^2$. The values shown in Fig. 2 were determined by the techniques discussed in this paper as well as by a contactless technique [14]. This data verifies that the effective emitter saturation current does scale inversely with the emitter area.

Minimizing the areas of the diffusions has several other beneficial effects beyond simply reducing the emitter component of the recombination. An evaluation of (2) for the case of an optimized solar cell (with A_n and A_p about 0.1 and $J_{on} = J_{op} = 4.5 \times 10^{-13}$ A/cm^2 [14]) indicates that for most illumination intensities, the emitter recombination dominates the device characteristic. Since the photogeneration is primarily in the front of the cell, the carriers must flow down a gradient in carrier density from the front of the cell to the back where they recombine. This gradient is significant at carrier densities above 10^{16} and must be accurately modeled for an accurate evaluation of the coefficients in (2). When this emitter recombination is minimized by reducing the area of the diffusions, the transport of carriers across the cell width for a given back surface carrier density is reduced. This effect is shown in Fig. 3 in which the carrier density across the cell in a line from the front surface to a p^+ depletion region edge at the back is plotted. This modeling result is a comparison of the carrier density profiles for a optimized point contact solar cell ($A_p = A_n = 0.1$) and for an Auger test structure of the geometry used in this study ($A_p = A_n = 0.0025$) as discussed in the next section. The deviation of the volume averaged carrier density from that which is determined from the terminal voltage at the back of the cell is greatly reduced in the Auger test structure.

Another more subtle effect of small-area diffusions is that the three-dimensional gradients in the cell near the diffusions are minimized by making the sizes of the diffused areas as small as possible even at a fixed coverage fraction (see the Appendix).

The relatively flat profile reduces the sensitivity of the extraction to the choice of device model or model parameters such as the diffusion coefficients and photogeneration profiles. Another way to reduce the difference in the average carrier density and the carrier density at the back of the cell, which is measured by the terminal voltage, is to make thin cells. In the limit of no emitter recombination and a very thin cell, then the extraction becomes independent of the both diffusion coefficient and the photogeneration profile because the carrier density will be uniform across the wafer.

The sensitivity of the device to the Auger recombination in particular is indicated in Fig. 4 in which the proportions of the various terms in (2) are displayed as a function of the incident intensity. This simulation is for an 86-μm-thick test structure as discussed in the next section. It is clear that the device will be dominated by the Auger recombination for incident power densities above 1.0 W/cm^2, a concentration of 10 suns. For high incident power densities, (2) is so strongly dominated by the Auger recombination term that it becomes essentially a one parameter curve fit for C_A. The parameters used in the modeling in this section are shown in Table II and are self-consistent with the conclusions of this paper.

The second diagnostic method that was used to determine the coefficients in (2) was the open-circuit voltage decay (OCVD) technique. Consider (1) and (2) after a forward bias excitation pulse is abruptly turned off. If the diffusion transit time is much smaller than the lifetime,

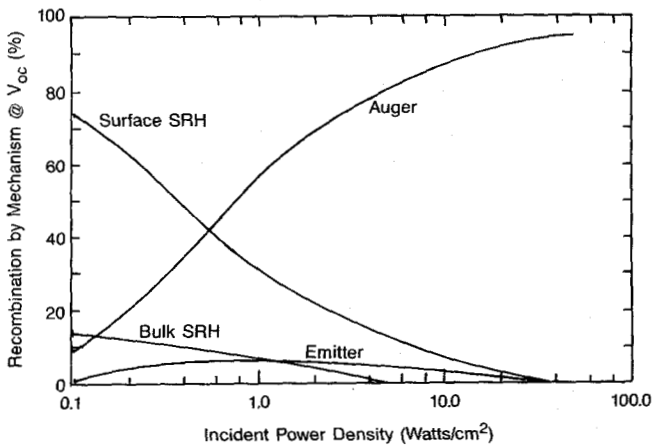

Fig. 4. The fraction of the total recombination contributed by each recombination component as a function of the illumination intensity for the device used in this study.

TABLE II
MODELING PARAMETERS

τ	3 milliseconds
S	7.5 cm/sec
J_{on}, J_{op}	4.5×10^{-13} Amps/cm^2
C_A	1.66×10^{-30} cm^6/sec
D_A	18 cm^2/sec [21,22]
n_i	$3.563 \times 10^{16}(T^{1.5})exp(-6980/T)$

the carrier density in the wafer will become constant across the wafer within a few transit times. From (1), the right side will then equal the change in carrier density with respect to time per unit area.

$$-qW\frac{dn}{dt} = \frac{q}{\tau}Wn + qS(n_f + n_b) + J_{on}A_n\left(\frac{n_n}{n_i}\right)^2 + J_{op}A_p\left(\frac{n_p}{n_i}\right)^2 + qWC_an^3. \quad (4)$$

But from (3)

$$\frac{dn}{dt} = n\frac{q}{2kT}\frac{dV}{dt}. \quad (5)$$

Hence

$$\frac{dV}{dt} = \frac{2kT}{qW}\left[\left(\frac{W}{\tau} + 2S\right) + \frac{(J_{on}A_n + J_{op}A_p)}{qn_i^2}n + C_AWn^2\right]. \quad (6)$$

A curve of dV_{oc}/dt versus V_{oc}, both experimental variables, can be converted to dV_{oc}/dt versus n using (3) (with a small three-dimensional correction shown in Fig. 5, derived in the Appendix) and fit to determine the coefficients of (6).

III. EXPERIMENT

The devices used in this study were fabricated using a self-aligned process sequence shown in Fig. 6 in order to achieve very small diffusion sizes. This fabrication schedule is similar to that previously described for optimized concentrator solar cells except that the oxide is not stripped after the diffusion drive-in step and later regrown as in that process [15]. The cells used in this study were 86 and 95 μm thick. Both devices had the same diffusion geometry for which the mask openings were 4 by 4 μm on a 100-μm square grid for both the phosphorus and the boron diffusions as shown in Fig. 7.

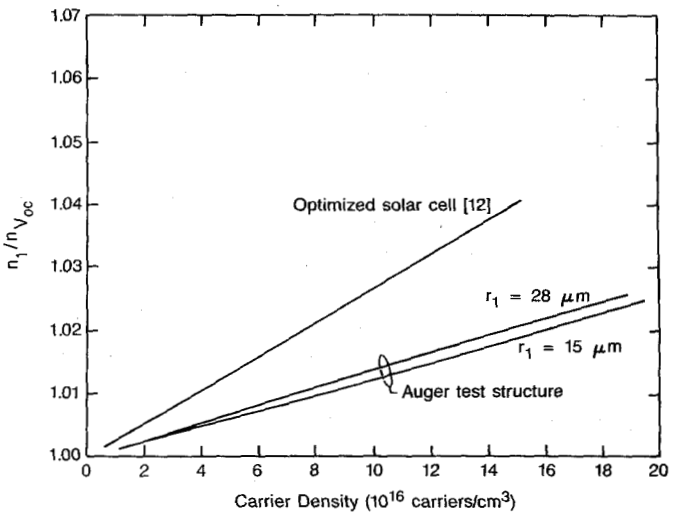

Fig. 5. The analytic correction to the back surface carrier density measured by the open-circuit voltage V_{oc}. This correction accounts for the three-dimensional gradients near each diffusion (Appendix).

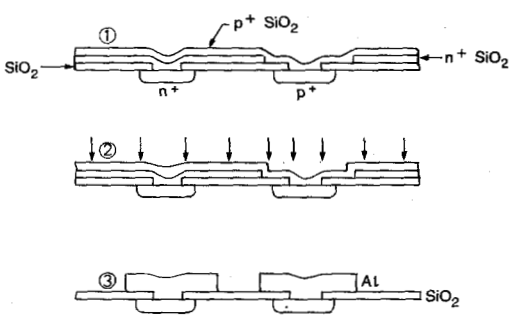

Fig. 6. A schematic diagram of the processing sequence for the devices used in this study. ① indicates the structure after the diffusions are driven in from B- and P-doped oxide sources. The doped oxides are stripped with an isotropic wet etch, ②, then the Al is deposited, annealed, and patterned. A similar process is described in more detail in [12].

The illuminated steady-state measurements of open-circuit voltage were performed in sunlight concentrated by front-surface mirrors as previously described [16]. The cell was tested under a low duty cycle in order to accurately control the cell temperature (a 0.005 duty cycle of 3-ms pulses). The range of incident power densities investigated was from 1 to 60 W/cm^3. During these measurements, the solar cell was clamped to a brass mount by a four-point voltage probe. The placement of the cell on the mount is accurate to within 100 μm in order to align the cell active area behind the 0.152-cm^2 aperture for the incoming sunlight. Data points at 0.1 W/cm^2 are

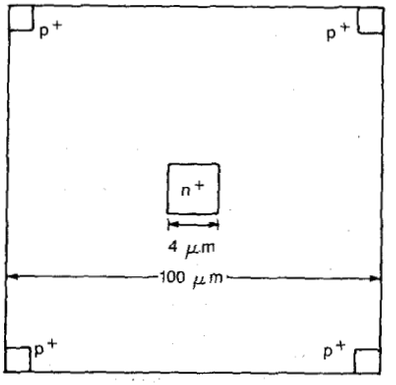

Fig. 7. A unit cell showing the diffusion mask geometry on the backside of the device. This unit cell is repeated to cover the entire 3 × 5 mm device. For comparison, the optimized solar cell reported in [12] has 10-μm emitters on a 50-μm pitch.

reported which were taken under an ASTM 86 Global spectrum at 25°C [17].

The OCVD measurements were performed under a 1/2000 duty cycle of 100-μs pulses of current that were used to forward bias the solar cell. The power supply switching was accomplished using a n-channel power MOSFET rated at 12-A continuous current. The open-circuit voltage decay was recorded on a digital oscilloscope for which the signal was averaged over 1000 traces. This curve was then fit to (6) to obtain the coefficients. The temperature of the mount was measured within 1 mm of the cell using a copper-constantin thermocouple (±0.5°C). By increasing the pulse length to 500 μs, which also increased the duty cycle by a factor of 5 the heating effects on the measurement could be evaluated. No effect on the resulting decay curve was observed (± 1 mV).

IV. Discussion

A curve of open-circuit voltage versus incident power density is shown in Fig. 8 comparing an 86-μm-thick Auger test structure with an optimized solar cell that had shown 27.5-percent efficiency at 10 W/cm^2 [12]. Compared to the baseline solar cell, the Auger test structure has higher voltages at each incident power. This is primarily due to the suppression of the emitter recombination accomplished by reducing the total area of the diffusions by a factor of 25. By using (3) in (2), the expected slope of the curve of V_{oc} versus ln (J_{ph}) can be found for cases in which the carrier densities are uniform across the wafer. A cell that is dominated by bulk and surface recombination, both linear in n, will increase 120 mV/decade of increase in J_{ph} at 300°C. Similarly, a characteristic dominated by the emitter and Auger recombination will give 60- and 40-mV/decade characteristics, respectively. The test structure characteristic approaches the 40 mV/decade expected for the Auger recombination at intensities greater than 10 W/cm^2. This is in good agreement with the modeling result shown in Fig. 4. The solar cell that had been optimized for maximum efficiency shows a characteristic closer to that expected for emitter

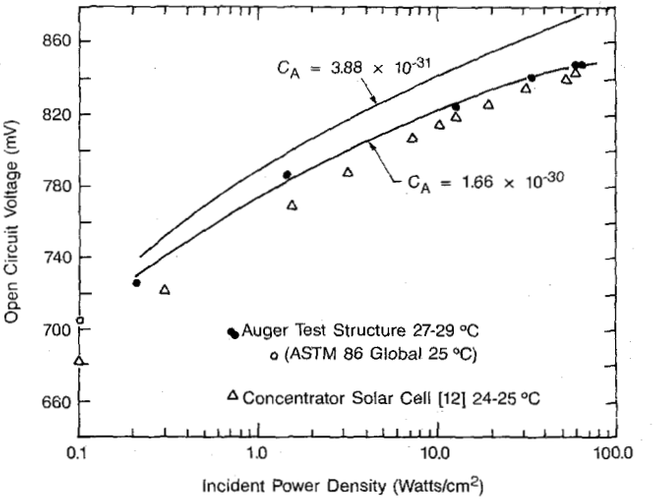

Fig. 8. The illuminated steady-state open-circuit voltage for an Auger test structure as a function of the incident illumination intensity. An optimized solar cell is shown for comparison. Modeling fits to the data from the Auger test structure for two choices of the Auger coefficient are shown.

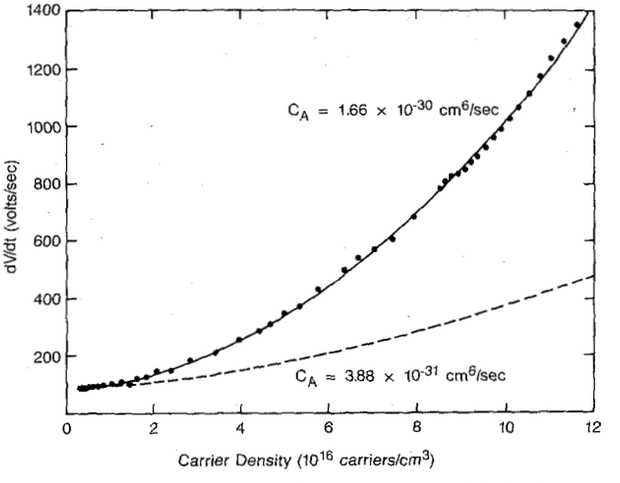

Fig. 9. The voltage decay rate as a function of the carrier density from an open-circuit voltage decay measurement. The upper curve is a modeling fit for C_A = 1.66 × 10^{-30} cm^6/s, the lower curve is for 3.8 × 10^{-31}.

recombination (60 mV/decade) for most of the measured range.

Two fits of the model to the data from the test structure are also shown in Fig. 8. The first shows a best fit of the three-dimensional model to the data using the coefficients listed in Table II. This curve is for an ambipolar Auger coefficient of 1.66 × 10^{-30} cm^6/s. An average of the Auger coefficient determined from 10 devices of the two different thicknesses shows a standard deviation of 4 percent. The second curve uses the most commonly referenced Auger coefficients from the literature, C_n = 2.8 × 10^{-31} and C_p = 0.99 × 10^{-31} cm^6/s [4].

A typical curve for the open-circuit voltage decay is shown in Fig. 9. The voltage has been converted to carrier density n using (2) with the three-dimensional correction of the emitter recombination current shown in Fig. 5 (see the Appendix). Several features are apparent. The slope

dV/dt becomes constant at low carrier densities showing the behavior expected from (6) since the surface and bulk recombination will dominate in this region. At the higher carrier densities the quadratic term, the Auger recombination, dominates. The term due to the emitter recombination, which would increase linearly with the carrier concentration, is very weak.

The best fits for these coefficients from five of the 86-μm devices yield an Auger coefficient of $1.65 \pm 0.08 \times 10^{-30}$ cm^6/s. The fit to four 95-μm devices is best for $1.67 \pm 0.04 \times 10^{-30}$ cm^6/s. These results are in excellent agreement with the steady-state results.

An interesting question brought up in recent publications is that the validity of (6) requires that the diffusion capacitance dominate over the junction capacitance in the voltage range of interest. This assumption has been shown to be in error in the case of typical silicon solar cells operating under low-level injection conditions [18], [19]. Due to the long carrier lifetimes and high-level injection, which increase the carrier storage, and the small diffusion coverage fraction, which decreases the junction capacitance, this condition is met in the devices considered here. At the lowest voltage used in this study, 600 mV or 1.5×10^{15} carriers/cm^3, the diffusion capacitance is more than five orders of magnitude greater than the junction capacitance.

Several sources of error should be mentioned for the present experiment. First, there are fundamental uncertainties in the determination of the carrier density from the terminal voltage. As discussed above, the device has been designed so that the terminal voltage indicates the bulk carrier density as closely as possible. However, the carrier density determined by this voltage depends critically on n_i, taken to be 1.45×10^{10} at 300 K in this experiment[1] (see Table II). The resulting Auger coefficient depends on n_i^3 in the steady-state illuminated open-circuit voltage measurement and n_i^2 in the OCVD experiment. The good agreement between the steady state and transient measurements is evidence that this value of n_i is accurate. A closely related error is the effect of an uncertainty in temperature on the extraction since the value of n_i changes about 6 percent/°C. For the steady-state illuminated experiment and an estimated experimental temperature uncertainty of 0.5°C, this represents a possibility of a 9-percent error in the extraction of the Auger coefficient.

Another possible source of error is a parasitic loss of carriers that was neglected in the analysis presented here for both the steady-state and OCVD measurements in the present experiment. This was the "perimeter" current, the carriers that diffuse out of the cell active area into the rest of the wafer where they recombine. These effects can be significant at the low carrier densities where the diffusion lengths are long [20]. This problem could be reduced by using larger devices than those used here, 3 by 5 mm, or by using different sized devices in order to extract this component. A numerical evaluation of this effect indicated that taking this into account would lower the extracted Auger coefficient by a maximum of 7 percent.

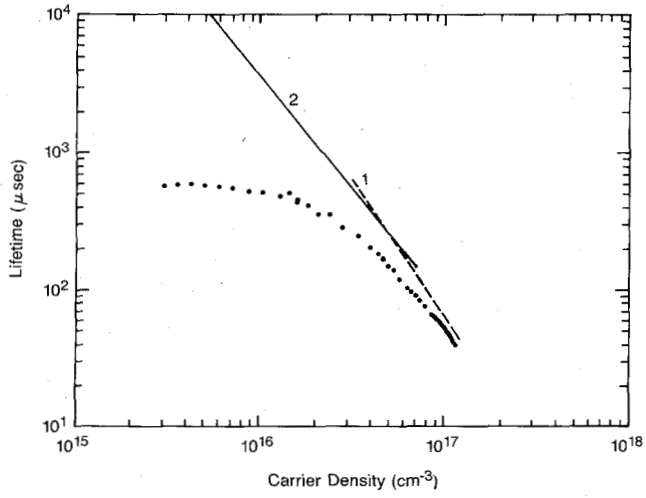

Fig. 10. A comparison of the lifetime results for highly injected silicon. The data from an OCVD trace are plotted here as lifetime versus carrier density. The dashed lines show the contribution attributed to Auger recombination from the present experiments (curve 1). Solid line 2 is a fit from [9].

The two most recent measurements of the Auger recombination as a function of injected carrier density are shown in Fig. 10. Some data from an open-circuit voltage decay trace of the Auger test structure is shown along with a curve of the Auger component extracted from this experiment. For the OCVD data shown, the lifetime was constructed from the voltage decay as

$$\tau_{\text{measured}} = \frac{2kT}{q(dV/dt)}. \tag{7}$$

The extracted curve assumes that the lifetime is inversely proportional to the carrier density squared. The other curve shown is from Yablonovitch and Gmitter and is fit to a -1.65 power rather than -2.0 [9]. Both of these curves are shown for the range in which they were fit to data. Because different slopes for the Auger recombination were assumed by Yablonovitch *et al.* and the present study, the two results correspond only at one carrier density, 4.5×10^{16} carriers/cm^3. These experiments were complimentary in that they were done in fundamentally different ways. In the experiment by Yablonovitch and Gmitter, the carrier density was determined based on the wafer conductivity. In the present experiment, the carrier density was determined from the terminal voltage.

Although the revised coefficient from our data is four times higher than those most commonly used in modeling, there is general agreement between the data from different authors on the lifetime for silicon with carrier densities in this range. The coefficients that Dziewior and Schimd derived from their data fit well only for their data points above 10^{18} carriers/cm^3 as noted in that paper. However,

[1] The activation energy of this expression was taken from H. D. Barber, "Effective mass and intrinsic concentration in silicon," *Solid-State Electron.*, vol. 10, pp. 1039–1051, 1967. The prefactor is a fit which gives the value at 300°C, 1.45×10^{10}/cm^3, commonly used in modeling.

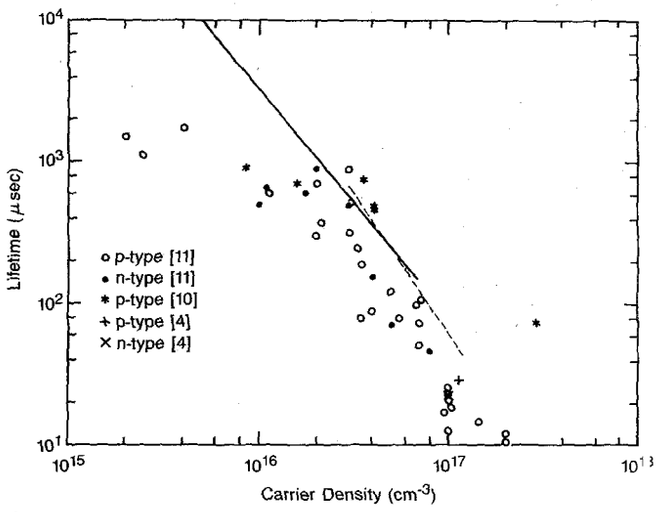

Fig. 11. A comparison of lifetimes measured in doped and undoped materials from the literature. The curves, from Fig. 10, show the Auger component of the lifetimes determined from highly injected silicon.

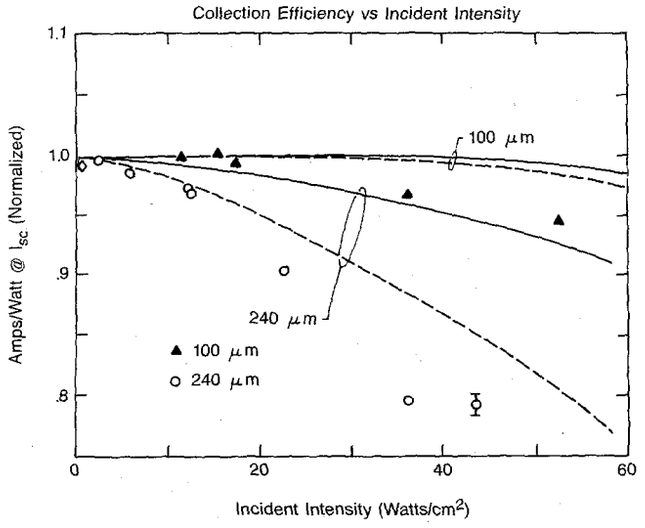

Fig. 12. The short-circuit current per incident watt of illumination for two thicknesses of solar cells [3]. The curves are normalized to be one at low intensities. The dashed curves are modeling fits for $C_A = 1.66 \times 10^{-30}$ cm^6/s, the solid curves are for 3.8×10^{-31}.

their data for lower carrier densities have *lower* lifetimes than the data presented here. A collection of data from several sources is shown in Fig. 11. This figure shows the lifetime data for Dziewior and Schmid in the range of lifetimes greater than 10 μs, as well as data taken from float-zone boules in the lower doping ranges [10], [11]. For highly injected silicon, the curves from Fig. 10 are also shown here. Additional data (not shown) has also indicated that the ambipolar Auger coefficient is between 1 and 2×10^{-30} cm^6/s [6]–[8] in the lower carrier density range.

It is interesting to plot this latest lifetime data from as-grown doped float-zone silicon in a comparison to the data from highly injected silicon. Huber *et al.* [11] measured lifetimes on doped float-zone silicon using the surface photovoltage method, shown here in Fig. 11, as well as by photoconductivity decay methods. It was noted that the photoconductivity measurements yield lifetimes two to three times longer. This conclusion indicates that if the lifetimes were reported from photoconductivity measurements, their p-type data would be in very good agreement with the p-type data from Ciszek [10] (measured by photoconductivity decay). The ambipolar lifetime deduced from these measurements on doped silicon

$$\frac{1}{\tau_{\text{ambipolar}}} \approx \frac{1}{\tau_p} + \frac{1}{\tau_n} \qquad (3)$$

is approaching the ambipolar lifetime measured in silicon, which is highly injected to the same carrier density. The recent results in undoped silicon have reduced the expected "fundamental" Auger lifetime as the lifetimes in doped silicon have steadily improved toward similar values. If this trend continues, then this agreement between data for highly injected and highly doped silicon would provide evidence for some mechanism that is independent of substrate doping type and depends only on the carrier concentrations.

Although some discussions of the physical mechanisms for the lifetime data at carrier densities less than 10^{18} carriers/cm^3, Fig. 11, exist in the literature, general agreement does not yet exist for the mechanisms of the recombination. In this paper, as in most others, the term Auger recombination is used to reference a recombination that produces a lifetime that depends on the carrier density products n^2p or p^2n. This is the only indication that this may be the mechanism involved as no stronger evidence that an Auger process is involved was presented here. Hence more fundamental studies are necessary to determine the mechanism for the apparent increased Auger coefficient at carrier densities lower than 10^{18}/cm^3.

In a previous paper in which the thickness dependence of the quantum efficiencies of optimized solar cells was discussed [3], discrepancies were seen between the modeled results, which used the Dziewior and Schmid coefficients, and the experimental results. The short-circuit current is another solar cell operating point for which the boundary conditions are especially well defined since the excess carrier density across the cell is then determined by the gradient caused by the particle current from the front to the back of the cell. This data of the relative quantum efficiencies at short-circuit current as a function of illumination intensity is shown in Fig. 12 with a comparison of modeling curves that use the different Auger coefficients. The Auger coefficients from the present experiment fit this data better than the coefficients previously used.

Fig. 12 demonstrates the importance of the Auger recombination to the modeling of the different operating points of optimized solar cells. The comparison of cells of different thicknesses highlights the fact that an accurate knowledge of this recombination is especially necessary when considering new cell geometries. Any geometry that results in high-peak carrier densities (as in thick cells) will become extremely sensitive to this recombination.

The carrier density range between 10^{16} and 2×10^{17} carriers/cm^3 is the range of interest in calculating the fundamental limits that this recombination places on Si solar cell efficiencies. A revision to the Auger coefficient in this range as presented here lowers the ultimate efficiencies possible for a highly idealized Si solar cell [2] by about 1 percent, to 36 percent. Using the existing technology and recombination parameters demonstrated in point-contact cells, the near term limit to the efficiency for this device appears to be 29 percent at 300°C. This is a conservative prediction based on the characteristics of the cells already demonstrated to be 27.5-percent efficient. The improved performance is foreseen in thinner cells, reasonably 70 μm, which would reduce the Auger recombination studied here. A less resistive metallization is also assumed [12].

V. Conclusions

A test structure has been designed and demonstrated that is optimized to study the Auger recombination in the carrier density range of interest to solar cell applications, 10^{16} to 2×10^{17} carriers/cm^3. Both a steady-state illuminated measurement and an open-circuit voltage decay measurement were used to extract the coefficient of the recombination, which goes as n^3. The resulting coefficient, 1.66×10^{-30} cm^6/s, is four times higher than that most commonly used in solar cell modeling. However, this result is shown to be in good agreement with data from the literature. Although the test structures used in this study are most similar to a solar cell under open-circuit conditions, the Auger coefficient determined from this study enables the quantum efficiency at short-circuit current of optimized point-contact cells to be modeled accurately. Prior to this study, the loss in quantum efficiency in these cells was considered to be anomalously high [3].

By generalizing the results from these recombination rates measured in highly injected silicon, it appears that the lifetimes in the very best quality doped material may already be approaching a fundamental limit. This would be evidence for a common recombination mechanism in the two cases, doped and highly injected materials. This data supports previous conclusions that the apparent Auger coefficients are much larger at carrier densities less than 10^{18}/cm^3 than at carrier densities greater than 10^{18} [6].

This result has several device implications. For power devices, the amount of conductivity modulation possible in highly injected regions is less than previously thought. Similar considerations will reduce the ultimate efficiency of solar cells by about 1 percent, to 36 percent at 300 K.

Appendix

The modeling used for the extraction of the recombination components in this paper closely follows the modeling of [13]. In that case, the cell was divided up into three regions shown in Fig. 13. In region 1, the carrier density was approximated by a one-dimensional solution. The carrier density was assumed to be constant in region 2. In region 3, a three-dimensional solution was used. If

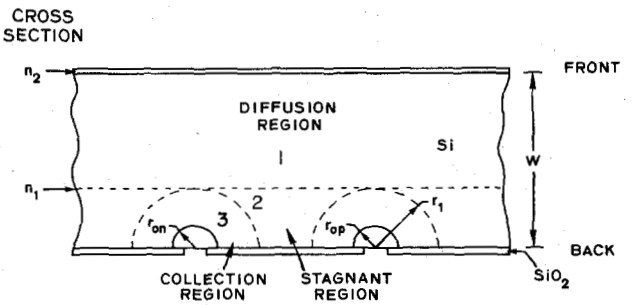

Fig. 13. A diagram showing the regions referred to in constructing an approximate three-dimensional model of the device.

the generation profile is assumed to be a delta function at the front of the cell and the diffusion lengthes are much longer than the cell thickness, then the solutions for Laplace's equation can be used to find the carrier densities. In this special case, the location of the boundary can be found by variational methods that determine the best solution of the diffusion equations for the entire device within these assumptions.

The approach used in this study was to use this same basic framework as a approximate analysis for the case of the open-circuit voltage, for which it does not rigorously apply when the bulk recombination is a significant fraction of the whole.

In the case of open circuit conditions, the diffusion in each of the three regions is ambipolar. The boundary, r_1 in Fig. 13, was chosen using the variational solution, which is only valid in the case of no recombination or generation in the bulk. This would be the case if the recombination were dominated by the emitter and the surface, and the photogeneration was entirely at the front of the cell. These were taken as boundary conditions in [13]. This same radius was used in this case because the profiles are so flat that the solutions are insensitive to the choice of r_1 within large bounds. The generation profile was not assumed to be a delta function at the front of the cell, but rather the combination of a uniform generation and a delta function that gives the same average depth of photogeneration as that determined by an integration over the absorption of the AM1.5 spectrum in silicon. Again the carrier density profile is so flat as to be extremely insensitive to this assumption.

A numerical integration was utilized in the one-dimensional regions to construct the carrier density in order to accurately account for the recombination due to the bulk terms in the integrals in (2). In the three-dimensional regions, the profiles were determined using an analytical solution assuming that the entire carrier flux were due to the electrons and holes that recombine in each emitter. This part of the modeling will be derived here because it differs from [13] in the case of the open-circuit voltage, and also because it was used apart from the modeling program as an explicit correction in the analysis of the OCVD data.

Experimentally, the p-type and n-type emitters in this study have been shown to have the same emitter satura-

tion currents ($J_{on} = 4.5 \times 10^{-13}$ A/cm^2), so in the case of the open-circuit voltage, they can be treated similarly. The flux of the electrons or holes that flows into the n^+ emitter is given by (expressed as a particle current)

$$J = J_{on}\left(\frac{n_{on}}{n_i}\right)^2\left(\frac{r_{on}}{r}\right)^2 \quad \text{for} \quad n_{on} \gg n_i \qquad (9)$$

where n_{on} is the carrier density in the base at the depletion region edge r_{on}. This radius r_{on} is for a hemisphere with an equivalent area to the n^+ diffused area. Integrating the diffusion equation

$$\int dn = \frac{1}{qD_A}\int J\, dr \qquad (10)$$

the drop in carrier density due to the gradient in the three dimensional region is found.

$$\Delta n = J_{on}\left(\frac{n_{on}}{n_i}\right)^2 \frac{r_{on}^2}{qD_A}\left(\frac{1}{r_{on}} - \frac{1}{r_1}\right). \qquad (11)$$

In these devices, the emitters only act as voltage "probes" to determine the carrier density. Equation (11) shows that because these diffused regions are also recombination sinks, they also perturb the carrier density by an amount Δn. Notice that this Δn decreases linearly with the junction radius r_{on} when this radius is much smaller than the boundary r_1. This indicates that the smallest possible emitters would be best for this study (we used 4 × 4 μm defined areas).

To find the carrier density at r_1 from the open-circuit voltage V_{oc}, this Δn must be taken into account. Since both emitters are the same radius and recombine equal numbers of carriers since they have the same emitter saturation currents

$$V_{oc} = 2kT \ln\left(\frac{n_1 - \Delta n}{n_i}\right) \qquad (12)$$

or

$$n_1 = \Delta n + n_i \exp\frac{qV_{oc}}{2kT}. \qquad (13)$$

This correction is contained within the solar cell modeling code that was used to fit the illuminated steady-state data. The code then constructs the one-dimensional solution for the carrier density up to the front surface accounting for the spatial dependence of the photogeneration profile and the carrier density dependences of the Auger recombination.

In the case of the OCVD measurements, the gradients in carrier density near the junction edges are assumed to create the only significant deviations from the flat profile across the cell shortly after the end of the forward-biasing pulse. Since these collection regions only contain a small fraction of the carriers in the cell, most of the recombination in the emitter region is supplied by carriers that diffuse through this region just as in the steady-state illuminated case. Therefore, (11) is a good approximation to the correction that should be made to the carrier density as determined from (3). Because of these gradients, a more accurate expression than (3) for the average carrier density n in the cell would be given by (13), where n_1 is taken to be the average carrier density in the cell. The correction due to the Δn is shown in Fig. 5 as the ratio of (13) to (3).

For the range of carrier densities used to fit (6) to find the recombination coefficients, up to 1.2×10^{17} carriers/cm^3, the largest correction to n is 1.6 percent for the devices in this study. The two curves shown for this device indicate the results from two different choices of the parameter r_1 to demonstrate the sensitivity to this parameter. Changing r_1 from 28 to 15 μm will alter the average carrier density by 0.2 percent. Since the coefficient C_A depends on n^2 in (5), the 0.2-percent difference in the correction to n would result in a difference of 0.4 percent in the extracted C_A.

Acknowledgment

The authors would like to thank Y. Kwark for the collaborations which contributed to the process schedules and devices reported here. Also thanks to S. Beckwith for process development, and D. Kane and E. Crabbé for many helpful discussions concerning this manuscript. D. Kane had initial data from another experiment that gave early support to these results.

References

[1] T. Tiedje, E. Yablonovitch, G. D. Cody, and B. G. Brooks, "Limiting efficiency of silicon solar cells," *IEEE Trans. Electron Devices*, vol. ED-31, pp. 711–761, 1984.

[2] P. Campbell and M. A. Green, "The limiting efficiency of silicon solar cells under concentrated sunlight," *IEEE Trans. Electron Devices*, vol. ED-33, no. 2, pp. 234–239, Feb. 1986.

[3] R. Sinton, Y. Kwark, P. Gruenbaum, R. M. Swanson, "Silicon point contact concentrator solar cells," in *Proc. 18th IEEE Photovoltaic Specialist Conf.*, pp. 61–65, Oct. 1985.

[4] J. Dziewior and W. Schmid, "Auger coefficients for highly doped and highly excited silicon," *Appl. Phys. Lett.*, vol. 31, no. 5, p. 346, 1977.

[5] K.G. Svantesson and N. G. Nilsson, "The temperature dependence of the Auger recombination coefficient of undoped silicon," *J. Phys. C*, vol. 12, p. 5111, 1979.

[6] Yu. Vaitkus and V. Grivitkas, "Dependence of the rate of interband Auger recombination on the carrier density in silicon," *Sov. Phys.—Semicond.*, vol. 15, no. 10, p. 1102, Oct. 1981.

[7] I. V. Grekhov and L. A. Delimova, "Auger recombination in silicon," *Sov. Phys.—Semicond.*, vol. 14, no. 5, p. 529, May 1980.

[8] L. A. Delimova, "Auger recombination in Si at low temperatures," *Sov. Phys.—Semicond.*, vol. 15, no. 7, p. 778, July 1981.

[9] E. Yablonovitch and T. Gmitter, "Auger recombination at low carrier densities," *Appl. Phys. Lett.*, vol. 49, no. 10, p. 587, Sept. 1986.

[10] T. F. Ciszek, "Material considerations for high-efficiency silicon solar cells," *Solar Cells*, May 1987.

[11] D. Huber, A. Bachmeier, T. Wahlich and H. Herzer, "Minority carrier diffusion length and doping density in nondegenerate silicon," in *Semiconductor Silicon 1986*, H. R. Huff, T. Abe, and B. Kobessen Eds., p. 1022, 1986.

[12] R. A. Sinton, Y. Kwark, J. Y. Gan, R. M. Swanson, "27.5% silicon concentrator solar cells," *IEEE Electron Device Lett.*, vol. EDL-7, no. 10, Oct. 1986.

[13] R. M. Swanson, "Point-contact solar cells; Modeling and experiment," *Solar Cells*, vol. 7, no. 1, 1986.

[14] D. E. Kane and R. M. Swanson, "Measurement of the emitter saturation current by a contactless photoconductivity decay method," in *Proc. IEEE 18th Photovoltaic Specialist Conf.*, p. 578, Oct. 1985.
[15] R. A. Sinton, Y. Kwark, S. Swirhun, and R. M. Swanson, "Silicon point contact concentrator solar cells," *IEEE Electron Device Lett.*, vol. EDL-6, no. 8, pp. 405–407, Aug. 1985.
[16] R. A. Crane, R. A. Sinton, R. R. King, and R. M. Swanson, "A high concentration solar cell test facility," in *Proc. IEEE 18th Photovoltaic Specialist Conf.*, pp. 963–966, Oct, 1985.
[17] K. Emery, measurement at Solar Energy Research Institute, Golden, CO, private communication.
[18] M. A. Green, "Minority carrier lifetimes using compensated differential open-circuit voltage decay," *Solid-State Electron.*, vol. 26, no. 11, p. 1117, 1983.
[19] F. A. Lindholm, J. J. Liou, A. Neugroschel, and T. W. Jung, "Improved determination of lifetime and surface reconvination velocity by observing transients," in *Proc. IEEE 18th Photovoltaic Specialist Conf.*, p. 611, Oct. 1985.
[20] R. A. Sinton, Y. Kwark, and R. M. Swanson, presented at the 14th Photovoltaic Concentrator Project Integration Meeting, Albuquerque, NM, June 4 and 5, 1985.
[21] I. V. Grekhov and L. A. Delimova, "Ambipolar diffusion coefficient in the case of electron-hole scattering in silicon," *Sov. Phys.—Semicond.*, vol. 14, no. 8, Aug. 1980.
[22] D. E. Kane and R. M. Swanson, to be published.

*

Ronald A. Sinton was born in Denver, CO, in February 1959. He received the B.S. degree in engineering physics from the University of Colorado, Boulder, in 1981. He is currently working toward the Ph.D. degree in applied physics at Stanford University. His research involves the development and device physics characterization of concentrator solar cells that operate under high-level injection conditions.

Richard M. Swanson (S'67–M'78) was born in Davenport, IA, on May 13, 1945. He received the B.S.E.E. and M.S.E.E. degrees from Ohio State University in 1969 and the Ph.D. degree from Stanford University in 1974. His dissertation research concerned the modeling and fabrication of complementary MOS integrated circuits for micropower applications and resulted in the theories and first experimental data on threshold adjustment by ion implantation and the operation of MOS transistors in the "weak inversion" regime. He was a National Science Foundation fellow while at Stanford.

While finishing his dissertation, he worked at Hewlett-Packard Laboratories, developing silicon-on-insulating-substrate technology. He received an IBM post-doctoral fellowship in 1974 at Stanford University to study techniques for solar-electric power generation. In 1976, he joined the faculty at Stanford as an Assistant Professor of Electrical Engineering and obtained funding from the Electric Power Research Institute to research thermophotovoltaic energy conversion for solar applications. Since then he has been actively involved in photovoltaics research. He is presently an Associate Professor of Electrical Engineering at Stanford University and heads a photovoltaics research team consisting of nine doctoral students, a research associate, an R&D engineer, and a processing technician. He has published over 50 technical papers.

Dr. Swanson is a member of the American Physical Society, the Electrochemical Society, the AAAS, the International Solar Energy Society, Sigma Chi, Tau Beta Pi, and Eta Kappa Nu.